Volume 1 | Number 1 | Jan 2013 | Pages 1–100

Journal of
Materials Chemistry A

Materials for energy and sustainability
www.rsc.org/materialsA

Li⁺

ROYAL SOCIETY
OF CHEMISTRY

ROYAL SOCIETY
OF CHEMISTRY

www.rsc.org/materialsA

TOC

Composite separator with ultra-thin ion exchangeable layer was developed to alleviating sever capacity decay of lithium ion batteries.
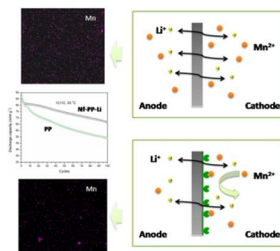
ARTICLE TYPE

Composite membrane with ultra-thin ion exchangeable functional layer: a new separator choice for manganese-based cathode material in lithium ion batteries

₅ **Junli Shi** [a], **Yonggao Xia**[*a], **Zhizhang Yuan** [b], **Huasheng Hu** [a], **Xianfeng Li**[*b], **Hui Jiang** [b], **Huamin Zhang** [b] and **Zhaoping Liu**[*a]

Composite membrane with ultra-thin ion exchangeable layer is specially designed as separator in lithium ion battery with manganese-based cathode material. The composite membrane features with Mn^{2+} capture
₁₀ function originated from the ion exchanging process, especially at high temperature, which is proved to help to alleviate the capacity decay of lithium ion batteries effectively. The enhanced thermal stability, improved wettability and higher lithium ion transference number of the composite membrane further suggest its promising application in the lithium ion batteries.

Introduction

₁₅ In the past several decades, the global energy source has long been the fossil fuels. However, this kind of energy source is facing to dry up. Research and development of the green, clean and sustainable energy systems has become the main direction of the world. [1] Lithium ion batteries as one of the most promising
₂₀ energy storage devices have attracted lots of attentions in recent years, due to their high power/energy density and long cycle life. [2, 3] Especially, lithium ion batteries containing manganese-based cathode materials, such as spinel $LiMn_2O_4$, layered $LiMn_{1/3}Ni_{1/3}Co_{1/3}O_2$, the Li-rich variants based cathodes and so
₂₅ on, have been widely studied and used. [4] These batteries feature with high security, low price and high specific energy, etc. However, there are still a few challenges when use them as the power sources for (hybrid) electric vehicles and for energy storage. Among these challenges, the Mn dissolution is a critical
₃₀ issue, which usually results in rapid capacity loss, especially when batteries are deposited at high temperature. [1-5]

The mechanism for the Mn dissolution is deemed as the disproportionation reaction of Mn^{3+} ($2Mn^{3+} \rightarrow Mn^{2+} + Mn^{4+}$) and the acid dissolution of Mn^{2+} caused by HF. HF is usually formed
₃₅ by the reaction of the $LiPF_6$ with the residual moisture in the electrolyte and the thermal decomposition of the $LiPF_6$. Dissolution of Mn^{2+} in the electrolyte would lead to a permanent loss of positive electrode materials. Meanwhile, the Mn^{2+} is found to be able to migrate to the negative electrode and to deposit on
₄₀ the electrode surface in the form of the metallic Mn clusters, which could prohibit the migration of lithium ions and destroy the solid electrolyte interphase (SEI) layer. So the batteries would show a serious irreversible capacity loss. [6, 7, 8, 9] To solve this problem, lots of efforts have been done in previous reports,
₄₅ including developing new stable lithium manganese based oxides, [10, 11] coating the lithium manganese based oxides with inorganic

materials or electrochemically active materials, [12, 13] introducing electrolyte addictives (tris(pentafluorophenyl)-borane (TPFPB), [14] heptamethyldisilazane, [15] etc.) to enhance the stability of the
₅₀ $LiPF_6$-based electrolytes and replacing the $LiPF_6$ with new non-fluorinated lithium salts. [16]

However, up to now, the inherent Mn dissolution phenomena still can not be completely overcame. In this case, how to further optimize the cycling performances and to alleviate the capacity
₅₅ decay of the manganese-based cathode materials in lithium ion batteries has become an important and critical issue not only for theoretical research but also for practical applications. [17] Recently, several works have reported the efforts to develop the lithiated ion exchangeable gel polymer electrolyte to improve the high
₆₀ temperature capacity retention of the $LiMn_2O_4$ based lithium ion batteries. [5, 18, 19] Nevertheless, limitations of these kinds of gel polymer electrolytes lie in that it is difficult to be scaled up and lies in their high cost.

In a different approach, this work developed a kind of
₆₅ composite separator with ultra-thin ion exchangeable layer on the surface of the traditional PP separator. This kind of separator features with relatively low cost, easily mass production and use. Meanwhile, the interlayer of the composite separator was kept with relatively high porosity to enable ion transportation, and the
₇₀ ultra-thin surface functional layer was kept dense to ensure the selectivity for Mn^{2+} and to realize the purpose of alleviating serious capacity decay of manganese-based cathode materials in lithium ion batteries. The properties and electrochemical performances of the composite membrane were illustrated
₇₅ detailedly.

Experimental methods

Materials

The PP separator (thickness: 20 μm) was supplied by Donghang Optoelectronics Technology Co., Ltd., China. Nafion dispersion
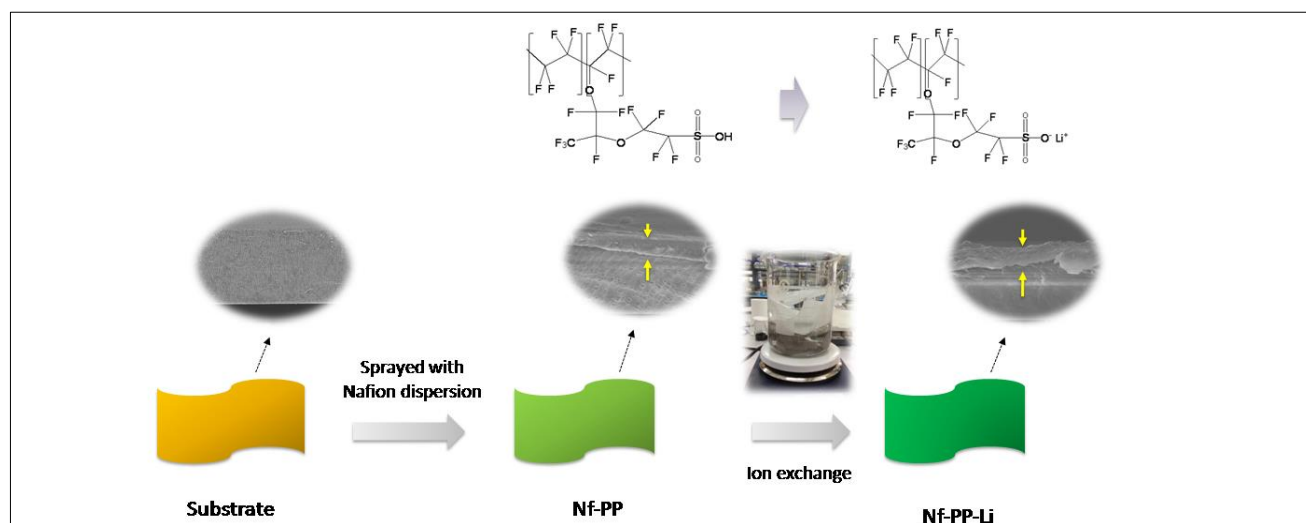
Scheme 1 Schematic illustration of the fabrication process of the ion exchangeable composite separator.

(D-520) and Nafion membrane 101 (thickness, 25 μm) were provided by DuPont App China Group Ltd. Isopropyl alcohol (IA) was purchased from Shanghai Chemical Reagents Co., China. The liquid electrolyte (S-3015A) is 1 M $LiPF_6$ in a mixture of ethylene carbonate and dimethyl carbonate (3:7 vol ratio), which was obtained from Zhangjiagang Guotai-Huarong New Chemical Materials Co., Ltd., China.

Fabrication of the ion exchangeable composite separator

To achieve the ion exchangeable composite separator, the ultra thin Nafion layer was introduced onto the PP separator. As a preparation step, the separator substrate was immersed in the IA bath for 0.5 h in advance. The 5.0 wt% Nafion dispersion was diluted with IA into 1.0 wt% solution. Then the solution was sprayed uniformly onto the separator substrate with an airbrush under the pressure of 0.2 MPa. After that, the obtained composite separator (coded as Nf-PP) was dipped into the LiOH · H_2O solution for 4 h for ion exchange at 80 °C. The LiOH · H_2O solution was prepared by dissolving 8.0 g LiOH · H_2O with 200 ml de-ionized water. After the separator was taken out, it was washed with de-ionized water until the wash water changed to be neutral. The separator after the ion exchange process was coded as Nf-PP-Li. The whole preparation process is illustrated as Scheme 1.

Characterization

After gold-spraying, separator morphology was characterized by field emission scanning electron microscopy (FESEM, S-4800, Hitachi, Japan). Attenuated total reflectance fourier transform infrared spectra (ATR-FTIR, Nicolet 6700, U.S.), X-ray Photoelectron Spectroscopy (XPS, AXIS UTLTRA DLD, Japan) and Energy dispersive X-ray spectroscopy (EDS, Quanta FEG 250, FEI) were used to characterize the surface chemical composition of the separators.

Thermal behaviors of the separators were determined with a differential scanning calorimeter (DSC, Perkin-Elmer, USA) and thermo gravimetric analyzer (TGA, Perkin-Elmer, USA) in a Al_2O_3 pan under an nitrogen atmosphere with a heating rate of 10 °C min^{-1}.
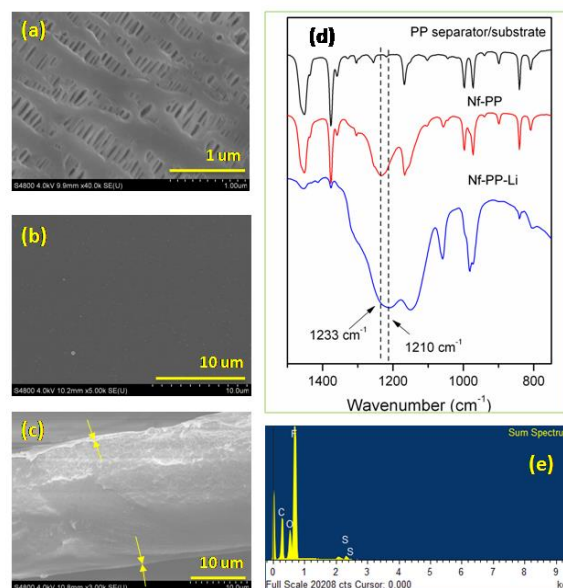
Fig. 1 The surface morphologies of (a) the PP separator substrate and (b) the Nf-PP-Li separator. (c) The cross-section SEM image of Nf-PP-Li. (d) The ATR-FTIR spectra of the PP separator, Nf-PP and Nf-PP-Li. (e) The EDS spectra of Nf-PP-Li.

The electrolyte uptake (ΔW) was determined according to the eqn (1):

$$\Delta W(\%)=(W\text{-}W_0)/W_0\times100 \qquad (1)$$

where W_0 and W is the weight of the dry membrane and wetted membrane, respectively.

The impedance spectra and potentiostatic current was determined on the electrochemical work station system (Solartron analytical, 1470E, Britain). The bulk impedance (R_b) was obtained with the assembly of stainless steel (SS)/ separator/ SS, and the interfacial resistance (R_{int}) and the potentiostatic current were obtained with the assembly of Li/ separator/ Li. The ion conductivity (σ) was calculated by the eqn (2):

$$\sigma=d/(R_b\times A) \qquad (2)$$

where d and A are the thickness and the effective area of the
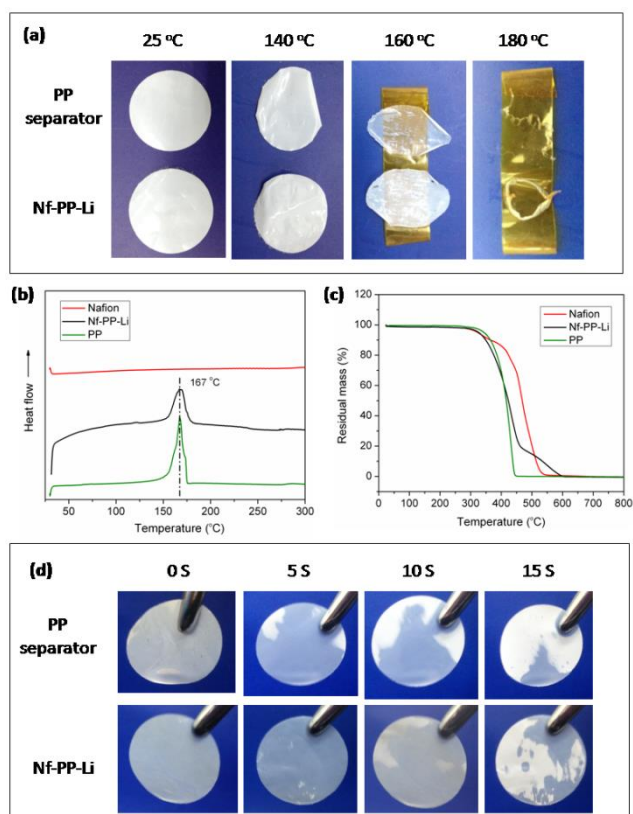
Fig. 2 (a) Thermal shrinkages of the Nf-PP-Li and PP separator after being treated at different temperatures. (b) The DSC curves of the PP, Nf-PP-Li and Nafion 101 membrane. (c) Thermal gravimetric analysis curves of the PP, Nf-PP-Li and Nafion 101
5 membrane. (d) The liquid electrolyte retention behavior of the Nf-PP-Li and PP separator.

separators, respectively. The transference number of lithium ions (t_+) was calculated according to the eqn (3):

10 $$t_+ = R_b/(V/I(\infty)-R_{int}) \qquad (3)$$

where V and $I(\infty)$ represent the voltage and quiescent current, respectively. And the $V/I(\infty)$ could be obtained from the slope of the I-V curve.

The cycling performances and the C-rate capacity were
15 determined on the LAND cell testing system (LAND CT2001A, China). For the half cells, they were cycled between 2.7 V and 4.3 V at 1 C. For the full cells, the voltage range is from 2.75 V to 4.2 V. The LiMn$_2$O$_4$ based cathode was prepared with LiMn$_2$O$_4$, super P and PVDF. The content of the LiMn$_2$O$_4$ was 85.0 wt%
20 for half cells and 95.5 wt% for full cells, respectively. And the LiMn$_2$O$_4$ content in each coin cell is about 5 mg for half cells and 17 mg for full cells, respectively. The interfacial resistance before and after the cycling process were also determined on the electrochemical work station system (Solartron analytical, 1470E,
25 Britain).

Results and discussion

SEM images of the PP separator substrate and the Nf-PP-Li separator are shown in Fig. 1. The commercialized PP separator was prepared via melt spinning and cold stretching method and
30 show a typical slit-like pore structure. The pore size is about 0.5
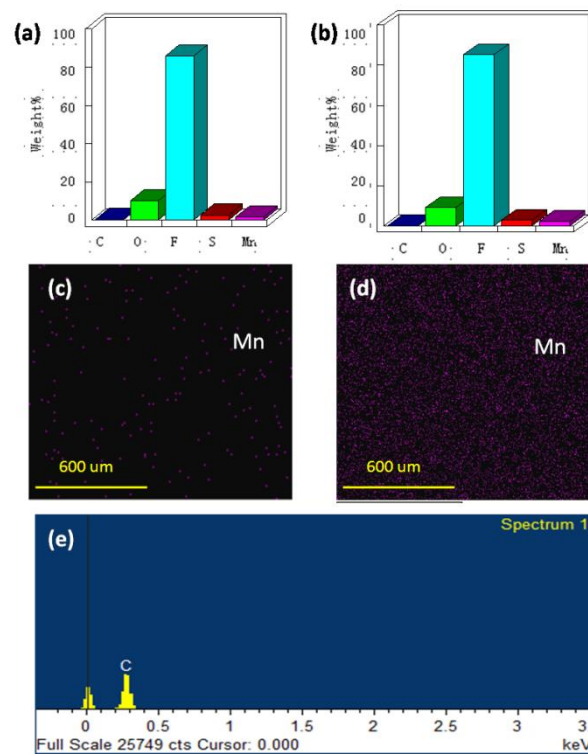
Fig. 3 EDS analysis (a) The mass content of the C, O, F, S and absorbed Mn^{2+} on the surface of Nf-PP-Li separator after being treated in the MnSO$_4$ solution for 24 h at 25 °C. (b) The mass content of the C, O, F, S and absorbed Mn^{2+} on the surface of Nf-
35 PP-Li after being treated in the MnSO$_4$ solution for 12 h at 55 °C. (c) EDS mapping analysis illustrating the distribution and concentration of Mn^{2+} on separator surface after being treated in the MnSO$_4$ solution for 24 h at 25 °C. (d) EDS mapping analysis illustrating the distribution and concentration of Mn^{2+} on
40 separator surface after being treated in the MnSO$_4$ solution for 12 h at 55 °C. (e) EDS spectra of PP separator after being treated on the MnSO$_4$ solution for 12 h at 55 °C.

μm. Through the spraying process and the lithiation process, an
45 ultra-thin functional layer was uniformly introduced onto the substrate (Fig. 1b and Fig. 1c). The thickness of the functional layer is about 0.6 μm.

Fig. 1d gives the ATR-FTIR spectra of the PP separator, Nf-PP separator and Nf-PP-Li separator. Introduction of the Nafion
50 layer creates a new adsorption peak at 1233 cm^{-1}, which corresponds to the characteristic peak of -SO$_3$H. After the lithiation process, obvious peak shift is observed. The adsorption peak at 1210 cm^{-1} is assigned to the characteristic peak of -SO$_3$Li, which indicates that Nf-PP-Li separator was successfully
55 prepared. Existence of Li$^+$ was further quantitatively characterized by XPS determination. As shown in Table 1, The Li$^+$ content on the surface layer of Nf-PP-Li separator is about 2.82 atom%, which is basically equal to the S content and 1/3 of the O content (Figure S1 and Table S1, Supporting information).
60 This result suggests that the lithiation reaction was effective and efficient. Besides, Fig 1e shows the EDS spectra of Nf-PP-Li separator. Appearance of the characteristic peaks of O, F and S

Table 1 The basic properties of the Nf-PP-Li separator and PP separator

Separator	Thickness (μm)	Li$^+$ content ^{a} (atom %)	Electrolyte uptake (wt %)	Retention ratio after 15 s (wt %)	σ (×10^{-4} S cm^{-1}, 25 ^{o}C)	t_+	Mn^{2+} concentration ^{b} (atom %)	
							25 ^{o}C for 24 h	55 ^{o}C for 12 h
Nf-PP-Li	21.2	2.82	143	72	0.42	0.74	0.49	1.13
PP	20.0	0.0	139	31	4.98	0.61	0.00	0.00

^{a} detected by XPS measurement.
^{b} detected by EDS measurement

element further confirms the successful preparation of the Nf-PP-Li separator.

Separators were deposited in the oven under different treatment temperatures for 1 h continuously to evaluate their thermal stability. The dimensional changes were recorded. As shown in Fig. 2a, compared with the Nf-PP-Li separator, PP separator shows more obvious shrinkage with increasing temperature. According to the DSC curves shown in Fig. 2b, the melting temperature of PP is around 167 ◦C. So the PP base separator would show serious shrinkage at around the melting point. But no obvious exothermic peak appears in the DSC curve of the Nafion material when the temperature is below 300 ^{o}C, indicating that the Nafion material owns superior thermal stability. [20] Besides, as can be seen in Fig. 3c, the PP separator, Nafion membrane and the Nf-PP-Li separator all owns high thermal decomposition temperature over 300 ^{o}C. [19] So the Nf-PP-Li separator exhibited better thermal stability. The enhanced thermal stability of the Nf-PP-Li is believed to make contribution to enhance the safety of the lithium ion batteries.

Better electrolyte wettability of separators has also long been pursued, which is beneficial for increasing the productivity and improving cycle performances of lithium ion batteries. [21] Especially, for the rapidly developing large-sized batteries, including (hybrid) electric vehicles and grid storage systems, the superior wettability of the entire separator is highly demanded. [22] Separators were immersed in the liquid electrolyte until being saturated. Then they were taken out in the glove box under argon atmosphere. The electrolyte uptake was firstly determined. As given in Table 1, the uptake amount for Nf-PP-Li separator (143 wt%) is slightly higher than that of the PP one (139 wt%). The slight increase in the uptake value is attributed to the Nafion-based coating layer, which could absorb a certain amount of liquid electrolyte. The affinity of separator with liquid electrolyte was evaluated by observing the evaporation of the liquid electrolyte from the separator. As shown in Fig. 2b, liquid electrolyte adsorbed on PP separator evaporates faster than that on the Nf-PP-Li separator. The determined retention ratio of the liquid electrolyte is 72% and 31% for the Nf-PP-Li separator and for the PP separator (Table 1), respectively. This is due to the intrinsically hydrophobicity and low surface energy of PP, yielding weak interaction, i. e. poor wettability, between the PP separator and the high polar liquid electrolyte. However, due to the unique chemical structure of the Nafion-based material, the interaction between Nf-PP-Li separator and liquid electrolyte was obviously enhanced.

The "Mn^{2+} capture" function of Nf-PP-Li separator was illustrated by immersing the separator in the MnSO$_4$ solution (4 g MnSO$_4$ dissolved in 150 ml deionized water) at different temperatures for different times. After being dried in the oven, separators were characterized by EDS measurement. Fig. 3a and Fig. 3b give the quantitative content of the Mn^{2+} on separator surface. The mass content and the atomic content of Mn^{2+} on the Nf-PP-Li separator after being treated in the MnSO$_4$ solution for 24 h at 25 ^{o}C is 1.41% and 0.49%, respectively (Fig 3a and Table 1), suggesting that the Nf-PP-Li could absorb the dissolved Mn^{2+}. This could be visually observed in Fig. 3c, in which the Mn^{2+} was marked as purple.

Considering the Mn dissolution would become more obvious at elevated temperature for the manganese-based cathode materials, the experiment at high temperature (55 ^{o}C) was also operated. The mass content and the atomic content of Mn^{2+} on the Nf-PP-Li separator after being treated in the MnSO$_4$ solution for 12 h at 55 ^{o}C is 3.35% and 1.13%, respectively (Fig 3b and Table 1). This result indicates that the Nf-PP-Li separator could capture much more Mn^{2+} at higher temperature. Fig. 3d gives same results, that more Mn^{2+} was detected on surface of the separator. The Nf-PP-Li separator with Mn^{2+} capture function is anticipated to be able to prevent the migration of Mn^{2+} from the cathode electrode to the anode electrode. So it is expected that the Nf-PP-Li separator is able to alleviate the sever capacity decay of the lithium ion batteries at high temperature, since Mn dissolution is more obvious under elevated temperature. [1-5] As a comparison, PP separator was treated under same conditions. The Mn^{2+} content was found to be 0.00% (Table 1 and Fig. 3e).

The Nf-PP-Li separator could be activated by liquid electrolyte and the electrochemical performances were further investigated. The ion conductivity of the Nf-PP-Li separator at room temperature is 0.42×10^{-4} S cm^{-1} (Table 1). The ion conductivity of the PP substrate at room temperature is 4.98×10^{-4} S cm^{-1}. Reduction of the ion conductivity is considered as the result of the introduction of the ion exchangeable functional layer, in which the migration of lithium ions is usually much slower than that in liquid electrolyte (i. e. the bulk resistance of the Nafion based material is much higher, as shown in Figure S2 and Figure S3, Supporting information). [5] However, the lithium ion transference number (t_+) of the Nf-PP-Li separator (0.74, Table 1) is higher than that of the PP substrate (0.61, Table 1), which is
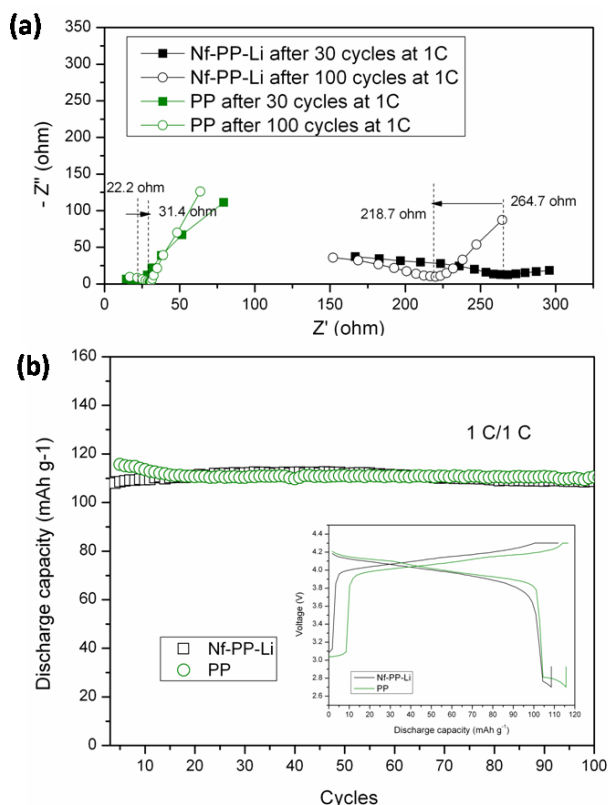
Fig. 4 (a) The variation of the interfacial resistance of the half cells containing the Nf-PP-Li separator and the PP separator before and after the cycling at 1 C. (b) The discharge capacity of the half cells containing the Nf-PP-Li separator and the PP separator at 1C. (The half cells were assembled with the $LiMn_2O_4$ cathode, separator and lithium anode.)

attributed to the contribution of the $-SO_3Li$. Since high lithium ion transference number has long been pursued, [19] preparation or introduction of the $-SO_3Li$ groups is proved to be able to provide an effective way and is expected to alleviated ion concentration gradients, decreasing internal resistance and alleviating interface polarization within lithium ion batteries. [23]

To explore the battery performances of the Nf-PP-Li separator, the cyclability and the interfacial properties of the half cells were firstly investigated. Due to the Mn dissolution phenomenon being more obvious and more serious for $LiMn_2O_4$, the $LiMn_2O_4$ was used as a representative for manganese-based cathode material to investigate the battery performances and the Mn dissolution behavior in the lithium ion batteries. The half cells were assembled with $LiMn_2O_4$ cathode, separator and lithium anode. The $LiMn_2O_4$ content in each coin cell is about 5 mg. As reported in previous works, [16] the pure Nafion membrane has very low ion conductivity (about 4.6×10^{-5} S cm^{-1}) and then showed poor cycling performances (Figure S4, Supporting information). Figure 4b shows the discharge capacity of the half cells containing Nf-PP-Li separators and PP separators as a function of the cycle number. The initial discharge capacity of the coin cells assembled with the Nf-PP-Li separator at 1 C is 110 mAh g^{-1}, which is a little lower than that of the cells containing the PP substrate (115 mAh g^{-1}, Fig. 4b inset). However, after 10 cycles, cells show similar discharge capacity (about 108 mAh g^{-1}).

Besides, during the 100 cycles, the cells containing the Nf-PP-Li separator show better cycling stability. For the Nf-PP-Li separator, the discharge capacity hardly changes at the 100th cycle. While the discharge capacity of the coin cells containing the PP separator at the 100th cycle decreases 4.7%. The discharge capacity of the coin cells containing the Nf-PP-Li separator was also compared with the commercial Celgard PP separator. In Qin et al's report, the discharge capacity of the coin cells containing Celgard PP separator (2500) at 0.5 C was about 90 mAh g^{-1}. [19] Through contrast analysis, the Nf-PP-Li separator still showed better battery performances.

It could be found that although the room temperature ion conductivity of the Nf-PP-Li separator is much lower than that of the PP separator (Table 1), better cyclability for the cells containing the Nf-PP-Li separator was obtained. The reason is attributed to higher lithium ion transference number, which means that much more lithium ions could participated the charge/discharge process effectively, and helps to create smaller cell polarization, yielding improved cyclability. [24] The results might indicate that the transference number is also an important influencing factor for cycling performances.

To achieve more comprehensive understanding for better cyclability of the Nf-PP-Li based cells. Variation of the interfacial resistance during the cycling process was tracked. As shown in Fig. 4a, the semicircle in the Nyquist plots represents the interfacial resistance. [25] The interfacial resistance of the cells containing the PP separator shows a little increase (from 22.2 ohm to 31.4 ohm) after 100 cycles. The reason is deemed to be the growth of the solid electrolyte interface (SEI) film. [26] But it is surprising that the interfacial resistance of the Nf-PP-Li based cells decreased during the 100 cycles. This behavior is expected to be the result of an enhanced charge transfer capacity in the interfacial layer from a direct involvement of the lithium ion desolvation and the increased SEI ion conductivity, which is originated from the unique chemical structure of the functional layer of the Nf-PP-Li separator. [27] The results suggest that the Nf-PP-Li is conducive to better interfacial property and then stable battery performances for the half cells.

Although Liu et al [5] have reported the application of the ion exchange membrane as electrolyte in $LiMn_2O_4$ based lithium ion batteries. They just investigated the battery performances of the $LiMn_2O_4$/lithium based half cells. However, the capacity decay is reported to be more serious for the full cells, since the reactions between the dissolved Mn^{2+} and the graphite anode, i. e. the reduction of Mn^{2+} into Mn metal on the surface of the graphite anode is one of the most important reasons for sever capacity fading, especially at high temperature. [1] Meanwhile, investigations on the battery performances of the full cells own more important guiding significance for practical application. So the effect of the Nf-PP-Li separator on battery performances was further investigated with the $LiMn_2O_4$/graphite based full cells.

Fig. 5a shows the initial discharging curves and the discharge capacity as a function of the cycle number of full cells containing the PP separator and the Nf-PP-Li separator at 25 °C. Same as the half cell, the full cells containing PP separator show a little higher initial discharge capacity (80.2 mAh g^{-1}) than that of the cells assembled with Nf-PP-Li separator (79.1 mAh g^{-1}) at 1 C. The capacity retention rate of the cells is similar for the 100 cycles
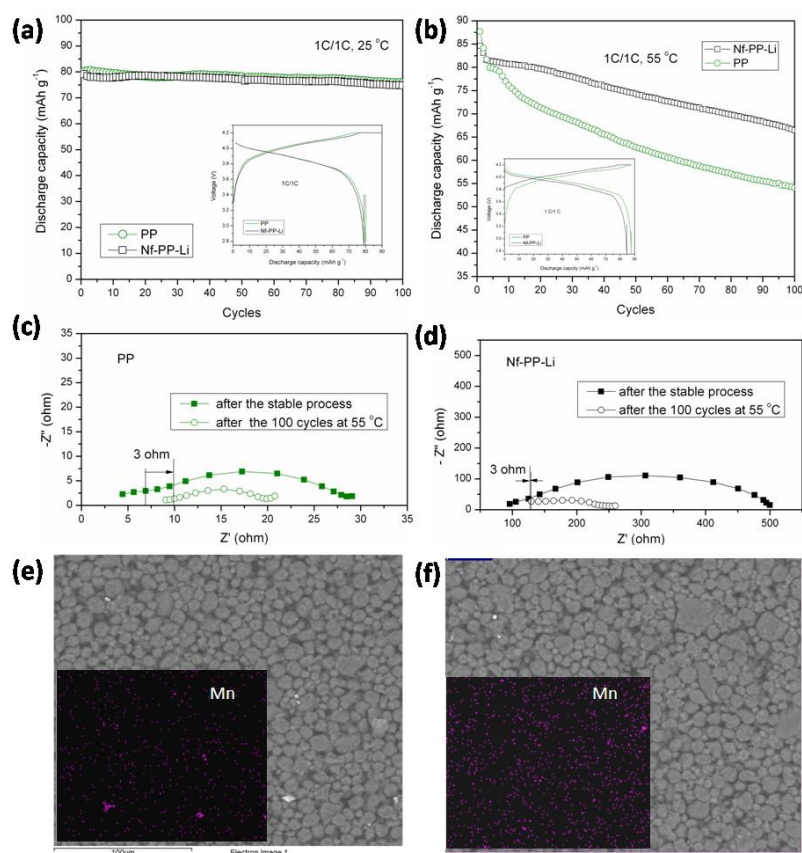
Fig. 5 The discharge capacity of the LiMn$_2$O$_4$/graphite based full cells containing the Nf-PP-Li separator and the PP separator at (a) 25 ^{o}C and (b) 55 ^{o}C. The charge/discharge current rate is 1 C. The inset is the initial discharging curves. (c-d) The variations of the interfacial resistances of the full cells containing the PP separator (c) and the Nf-PP-Li separator (d) before and after the cycling at 55 ^{o}C.The SEM of the anodes of the cells containing (e) Nf-PP-Li separator and (f) PP separator after the cycling process at 55 ^{o}C. EDS images depicting the distribution and the concentration of the Mn element (inset).

(about 94.5%). That is to say that there is little difference for battery performances of the full cells containing the PP separator and the Nf-PP-Li separator at 25 ^{o}C, which might be the result of the relatively stable structure of the LiMn$_2$O$_4$ and the unapparent Mn dissolution phenomenon at room temperature for the first 100 cycles at 1 C.

Relatively lower discharge capacities of the full cells than that of the half cells are ascribe to different anodes and different LiMn$_2$O$_4$ contents in the coin cells. When the graphite was used as anodes, irreversible intercalation/de-intercalation of lithium ions in/from the anode caused a decrease of the discharge capacity. [28] Besides, to analyze the cycle performances and the Mn dissolution phenomenon of the full cells, the electrochemical performances were determined under harsher operating conditions (i. e. the high-mass-loading electrodes, about 17 mg LiMn$_2$O$_4$ in each coin cell). [28] So the determined discharge capacities of the full cells are obviously lower than that of the half cells.

The cycle performances at high temperature (55 ^{o}C) were further investigated. As shown in Fig. 5b, the initial discharge capacity at 1 C of the cells containing the PP separator and the Nf-PP-Li separator is 87.6 mAh g^{-1} and 84.6 mAh g^{-1}, respectively. Higher initial discharge capacity for cells containing PP separator comes from higher ion conduction ability for PP separator (Table 1). However, severer capacity decay was found

for the PP separator based full cells. After 100 cycles at 1 C and 55 ^{o}C, the capacity retention rate for the full cells containing the PP separator and the Nf-PP-Li separator is 61.7% and 78.6%, respectively. Generally, the discharge capacity decay at high temperature is considered to be the result of the LiPF$_6$ based electrolyte decomposition at temperature higher than 55 ^{o}C and Mn dissolution. [5, 29] The enhanced stability of the cycling performances for the full cells containing the Nf-PP-Li separator is deem to come from the following reasons. Firstly, better wettability for Nf-PP-Li separator could yield stronger adhesion for the electrodes and a uniformly wetted interfacial layer in the full cells, which could help to mitigate the unwanted side reaction between the liquid electrolyte and the electrodes, yielding better cell performance. [28] Secondly, as discussed above, the Nf-PP-Li separator owns the Mn^{2+} capture function. So it is expected that during the cycling process, ion exchange will occur between the dissolved Mn^{2+} from the cathode and the –SO$_3$Li groups in the dense surface layer of the Nf-PP-Li separator, due to stronger interaction between the –SO$_3^-$ and the Mn^{2+}. [1] This implies that the Mn^{2+} could be bounded to the separator and that the reduction of the Mn^{2+} into Mn metal on the graphite anode could be effectively prohibited. Meanwhile, the ion conduction ability of the Nf-PP-Li separator before and after the ion exchange process changes little (Figure S2, Supporting information), resulting in improved battery performances and higher capacity retention rate after 100 cycles. The variations of the interfacial resistances

before and after the cycling process were shown in Fig. 5c and Fig. 5d, which show little differences for the Nf-PP-Li separator based full cells and for the PP separator based full cells. The reason is not completely understood and would be further
5 explored.

The deduction on Mn^{2+} capture behavior of the Nf-PP-Li separator during the cycling process was further proved by investigating the distribution and concentration of the Mn element on the surface of the anodes after the full cells were
10 cycled for 100 cycles at 55 °C. Compared with EDS image of the Mn element in the cells containing the PP separator (labeled as purple, Fig. 5f), the full cells with the Nf-PP-Li separator show an obviously lower Mn concentration on the surface of the anode (labeled as purple, Fig. 5e), implying lower Mn metal byproducts
15 being formed. This result supports the explanation for the improved cycling capacity of the $LiMn_2O_4$ based full cells and the validity of the ion exchangeable composite separator. However, it must be admitted that the performances of the composite separator were still not optimal, for example, the ion
20 conductivity is relatively low and there are still capacity decay for the full cells containing the composite separator. As a promising attempt to overcome the above problems, introduction of an ultra-thin functional layer with higher ion conduction ability and higher Mn^{2+} adsorption capacity could be proposed. The main
25 contribution of this work is providing a new separator concept to alleviate severe capacity decay of the manganese-based cathode materials in lithium ion batteries.

Conclusions

A kind of composite separator (Nf-PP-Li) with ultra-thin ion
30 exchangeable layer was successfully prepared by introducing the lithiated Nafion layer. Comparing with the PP separator, the thermal stability and the wettability of the Nf-PP-Li separator were both enhanced. Basing on the Mn^{2+} capture function originated from the ion exchanging between the $-SO_3Li$ group
35 and Mn^{2+}, the sever capacity decay of the $LiMn_2O_4$ based full cells at 55 °C was effectively alleviated. Since the Mn dissolution is a universal phenomenon for lithium ion batteries with manganese-based cathode materials, it is anticipated that the composite separator could be extend to the application for other
40 manganese based cathode materials.

Acknowledgements

Notes and references

[a] *Ningbo Institute of Materials Technology Engineering (NIMTE),*
50 *Chinese Academy of Sciences, Zhejiang, China, 31520. Fax: +86-574-86324027; Tel: +86-574- 86324027; E-mail: xiayg@nimte.ac.cn; liuzp@nimte.ac.cn*
[b] *Division of energy storage, Dalian Institute of Chemical Physics, Chinese Academy of Sciences, Dalian, China, 116023. Fax: +86-411-*
55 *84379669; Tel: +86-411-84379669; E-mail: lixianfeng@dicp.ac.cn*

† Electronic Supplementary Information (ESI) available: [XPS spectra of the composite separator (Figure S1); The atomic concentration of the composite separator determined by XPS (Table S1); The Nyquist plots of the Nf-PP-Li separator before and after the ion exchange process (Figure
60 S2); The Nyquist plots of the Nafion membrane (Figure S3); The discharge capacity and coulombic efficiency of the coin cells containing the Nafion membrane (Figure S4)]. See DOI: 10.1039/b000000x/

1　S. H. Woo, H. W. Lim, S. Jeon, J. J. Travis, S. M. George, S. H. Lee, Y. N. Jo, J. H. Song, Y. S. Jung, S. Y. Hong, N. S. Choi and K. T. Lee, *J. Electrochem. Soc.*, 2013, **160**, A2234.
2　J. J. Zhang, L. P. Yue, Q. S. Kong, Z. H. Liu, X. H. Zhou, C. J. Zhang, Q. Xu, B. Zhang, G. L. Ding, B. S. Qin, Y. L. Duan, Q. F. Wang, J. H. Yao, G. L. Cui and L. Q. Chen, *Sci. Rep.,* 2014, **4**, 3935.
3　C. J. Orendorff, T. N. Lambert, C. A. Chavez, M. Bencomo and K. R. Fenton, *Adv. Energy Mater.*, 2013, **3**, 314.
4　X. C. Xiao, D. Ahn, Z. Y. Liu, J. H. Kim, P. Lu, *Electrochem. Commun.*, 2013, **32**, 31.
5　Y. B. Liu, L. Tan and L. Li, *Chem. Commun.*, 2012, **48**, 9858.
6　J. S. Kim, K. S. Kim, W. Cho, W. H. Shin, R. Kanno and J. W. Choi, *Nano Lett.*, 2012, **12**, 6358.
7　R. Dedryvère, D. Foix, S. Franger, S. Patoux, L. Daniel and D. Gonbeau, *J. Phys. Chem. C*, 2010, **114**, 10999.
8　M. Hirayama, H. Ido, K. S. Kim, W. Cho, K. Tamura, J. Mizuki and R. Kanno, *J. Am. Chem. Soc.*, 2010, **132**, 15268.
9　M. J. Lee, S. Lee, P. Oh, Y. Kim and J. Cho, *Nano Lett.*, 2014, **14**, 993.
10　M. S. Whittingham, *Chem. Rev.*, 2004, **104**, 4271.
11　G. G. Amatucci, N. Pereira, T. Zheng and J. M. Tarascon, *J. Electrochem. Soc.*, 2001, **148**, 171.
12　S. Lee, Y. Cho, H. K. Song, K. L. Lee, J. Cho, *J. Angew. Chem. Int. Ed.*, 2012, **51**, 8748.
13　S. T. Myung, K. S. Lee, D. W. Kim, B. Scrosati, Y. K. Sun, Energy Environ. Sci. 2011, 4, 935-939.
14　X. Sun, H. S. Lee, X. Q. Yang and J. McBreen, Electrochem. *Solid State Lett.*, 2002, **5**, 248.
15　Y. Li, R. Zhang, J. Liu and C. Yang, *J. Power Sources*, 2009, **189**, 685.
16　Z. Cai, Y. Liu, S. Liu, L. Li and Y. Zhang, *Energy Environ. Sci.*, 2012, **5**, 5690.
17　K. W. Leitner, H. Wolf, A. Garsuch, F. Chesneau, M. Schulz-Dobrick, *J. Power Sources*, 2013, **244**, 548.
18　Z. J. Cai, Y. B. Liu, S. S. Liu, L. Li and Y. M. Zhang, *Energy Environ. Sci.*, 2012, **5**, 5690.
19　B. Qin, Z. Liu, G. Ding, Y. Duan, C. Zhang and G. Cui, *Electrochim. Acta*, 2014, **141**, 167.
20　X. Zhou, L. Yue, J. Zhang, and G. Cui, *J. Electrochem. Soc.*, 2013, **160**, A1341.
21　M. H. Ryou, Y. M. Lee, J. K. Park and J. W. Choi, *Adv. Mater.*, 2011, **23**, 3066.
22　J. H. Kim, J. H. Kim, E. S. Choi, H. K. Yu, J. H. Kim, Q. Wu, S. J. Chun, S. Y. Lee and S. Y. Lee, *J. Power Sources*, 2013, **242**, 533.
23　M. M. Hiller, M. Joost, H. J. Gores, S. Passerini and H. D. Wiemhöfer, *Electrochim. Acta*, 2013, **114**, 21.
24　J. L. Schaefer , D. A. Yanga , and L. A. Archer, *Chem. Mater.*, 2013, **25**, 834.
25　C. Z. Man, P. Jiang, K. W. Wong, Y. Zhao, C. Y. Tang, M. K. Fan, W. M. Lau, J. Mei, S. M. Li, H. Liu and D. Hui, *J. Mater. Chem. A*, 2014, **2**, 11980.
26　M. Yanilmaz, Y. Lu, M. Dirican, K. Fu, X. W. Zhang, *J. Membrane Sci.*, 2014, **456**, 57.
27　O. Borodin and D. Bedrov, *J. Phys. Chem. C*, 2014, **118**, 18362.
28　J. H. Kim, J. H. Kim, K. H. Choi, H. K. Yu, J. H. Kim, J. S. Lee and S. Y. Lee, *Nano Lett.*, 2014, **14**, 4438.
29　K. Y. Chung and K. B. Kim, *Electrochim. Acta*, 2004, **49**, 3327.